CHEMISTRY OF MATERIALS

ARTICLE

pubs.acs.org/cm

Bifunctional Core−Shell−Corona Particles for Amphiphobic Coatings

Dean Xiong,[†] Guojun Liu,[†,*] Jiguang Zhang,[†] and Scott Duncan[‡]

[†]Department of Chemistry, Queen's University, 90 Bader Lane, Kingston, Ontario, Canada K7L 3N6

[‡]Department of National Defence, Defence R&D Canada Suffield, Box 4000 Stn Main, Medicine Hat, Alberta, Canada T1A 8K6

ABSTRACT: Bifunctional core−shell−corona particles that bore both fluorinated units and hydroxyl groups in the corona were synthesized. The core particles were prepared from monomer methyl methacrylate (MMA) and cross-linker ethylene glycol dimethacrylate (EGDMA). The shell was grown from MMA, EGDMA, and HEA-Cl [2-(2′-chloropropionato)-ethyl acrylate] via seeded emulsion polymerization. The incorporated HEA-Cl groups initiated the atom-transfer radical polymerization of 2-hydroxyethyl acrylate (HEA) to produce a PHEA corona. Particles with both fluorinated units and hydroxyl groups in the corona were obtained after reacting ∼80% of the PHEA hydroxyl groups with perfluorononanoyl chloride. After casting trifluorotoluene dispersions of these particles onto a glass plate, the resultant coating was amphiphobic, possessing high contact angles for both water and diodomethane. For water, the advancing contact angle reached 165° and the advancing and receding angle difference (hysteresis) was small. Thus, the coating was superhydrophobic. More interestingly, the hydroxyl groups in the particle coronas could be used to bond with an epoxy glue, which adhered to glass substrate, to yield a "permanent" amphiphobic coating.

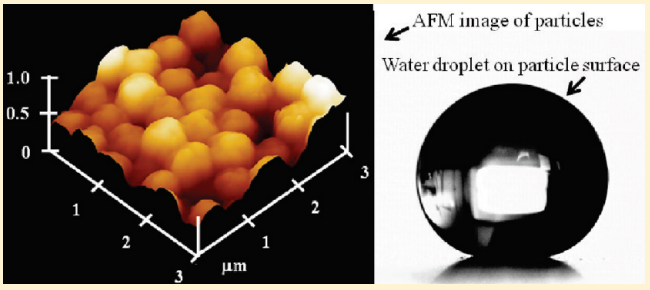

KEYWORDS: superhydrophobic coatings, fluorinated particles, bifunctional particles, emulsion polymerization, atom transfer radical polymerization, particle binding, and epoxy glue

I. INTRODUCTION

Fluorinated polymers are interesting, because of their water and oil repellence,[1,2] low dielectric constants and refractive indices,[3,4] excellent chemical and thermal stability,[5,6] and solubility in supercritical CO_2.[7] Among these properties, the low surface energy of fluorinated polymers, and thus their water and oil repellence and self-cleaning capabilities are the most interesting.

Studies of natural superhydrophobic surfaces, such as lotus leaves[8,9] and water strider legs,[10] have helped shed light on the essential criteria for superhydrophobicity in particular and superamphiphobicity (high repellence of both oil and water) in general. Aside from a low surface tension, the surfaces should also be rough to render superamphiphobicity or the self-cleaning properties.[11−14] While many exotic methods,[15−17] as well as lithography,[13,18,19] have been used to prepare rough surfaces, a more practical and less-expensive way might be to apply a rough coating onto a substrate. This can be achieved using traditional coating techniques, such as dry powder coating[20] or wet painting. In wet painting, nondeformable particles with fluorinated surfaces may be added into a paint mixture consisting of the binder (resin), vehicle (solvent), and other additives. After the solvent evaporates, the binder will hopefully form a uniform film strewn with the fluorinated particles, which tower above the binding film. Therefore, the use of fluorinated particles may provide a viable approach toward composite rough coatings.[21,22]

The above prospect has propelled many publications on fluorinated particles.[23,24] For example, core−shell (CS) particles with a fluorinated shell have been prepared via seeded emulsion polymerization, using nanosized silica particles as the seeds.[25] The reaction between calcium chloride and sodium carbonate in the presence of fluoroalkyl end-capped acrylic acid allowed the preparation of fluorinated calcium carbonate particles.[26] Silica and alumina particles were fluorinated via surface functionalization using perfluoroalkyl chlorosilane.[27] Furthermore, the reduction of gold ions by poly(methylhydrosiloxane) in the presence of fluoroalkyl end-capped co-oligomeric nanoparticles yielded a novel class of fluorinated co-oligomeric nanocomposite-encapsulated gold nanoparticles.[28]

Despite past efforts, prior particles were designed and prepared with little consideration imparted to the final integration of the particles into a durable rough coating. Fluorinated particles do not stick to hydrocarbon polymers. A durable coating is possible only if there is strong particle/resin interaction, as well as resin/substrate interaction. Reported in this paper are the design and preparation of bifunctional particles that possess surface fluorinated groups and hydroxyl groups. The latter should bond covalently with epoxy or polyurethane glues, which have been shown to bond with the hydroxyl groups of fluorinated polyols to yield amphiphobic fluorinated polyurethane coatings.[29,30]

Scheme 1 illustrates our approach to these particles with bifunctional surfaces. These particles have a core−shell−corona (CSC) structure. The core emerged from the surfactant-free

Received: December 27, 2010
Revised: May 9, 2011
Published: May 19, 2011

Scheme 1. Approach for Core−Shell−Corona (CSC) Microsphere Preparation[a]

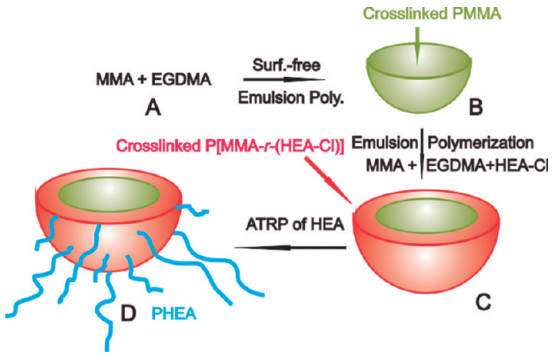

[a] Only halves of the spheres are shown to reveal the internal structures of the spheres.

emulsion polymerization of the monomer methyl methacrylate (MMA) and the cross-linker ethylene glycol dimethacrylate (EGDMA) (A→B). The shell grew on the core from the semicontinuous seeded emulsion polymerization of MMA, EGDMA, and HEA-Cl [2-(2′-chloropropionato)ethyl acrylate] (B→C). The incorporated HEA-Cl groups then initiated the atom transfer radical polymerization (ATRP) of 2-hydroxyethyl acrylate (HEA) to spring up a PHEA corona (C→D). A bifunctional corona was procured after reacting ∼80% of the PHEA hydroxyl groups with perfluorononanoyl chloride.

While we believe that emulsion polymerization, ATRP, and surface functionalization have never been combined to prepare fluorinated particles, the combination of emulsion polymerization and ATRP has been used to prepare other particles.[31−34] Charleux and co-workers[35] and Brooks and co-workers[36] used this combination to prepare particles that had a hydrophobic core and a hydrophilic corona. Based on a slight variation, Stover and co-workers[31] combined precipitation polymerization and ATRP to prepare particles that were supposedly better scaffolds for catalysts and reagents. Aside from the emulsion polymerization and ATRP approach, much smaller CSC particles can also be created from self-assembling and chemically processing ABC triblock copolymers.[37−39]

II. EXPERIMENTAL SECTION

Materials. The monomers 2-hydroxyethyl acrylate (HEA, 96%), methyl methacrylate (MMA, 99%), and ethylene glycol dimethacrylate (EGDMA, 96%) were purchased from Aldrich and were distilled under reduced pressure before use. Literature procedures were followed for the synthesis of 2-(2′-chloropropionato)ethyl acrylate (CH_2═$CHCOO(CH_2)_2OOCCHClCH_3$, HEA-Cl)[40] and tris[2-(dimethylamino)ethyl]-amine (Me_6TREN).[41] 2,2-Azobisisobutyronitrile (AIBN) (Fisher Scientific) was recrystallized from ethanol before use. 2-Chloropropionyl chloride (97%), triethylamine (99%), perfluorononanoyl chloride ($CF_3(CF_2)_7COCl$, 98%), potassium persulfate, CuBr, $CuBr_2$, and methyl 2-chloropropinate were purchased from Aldrich, and were used as received. The epoxy glue used was of the Varian Torr Seal brand. It consisted of two parts: Part A most likely consisted of the glycidyl moieties, plasticizer, and silica, and Part B most likely consisted of diamines. The cure times were specified as 24 h at 25 °C and 2 h at 60 °C.

Core−Shell Particles. To synthesize the cores of the CS particles, 4.80 g (48.0 mmol) of MMA, 0.40 g (2.0 mmol) of EGDMA, and 41 mg (0.15 μmol) of potassium persulfate in 5.0 mL of water were mixed under stirring (600 rpm) with 130 mL of deionized water in a 500-mL three-necked round-bottom flask at room temperature. The mixture was bubbled with nitrogen for 15 min before the flask, under N_2 protection, was immersed into an oil bath that was preheated to 90 °C. This temperature was maintained for 2 h to complete the polymerization.

From the resultant mixture, 43 mL was removed using a syringe and added into a 250-mL three-necked round-bottom flask that was filled with N_2. This was followed by the addition of 2.4 mg (14.6 μmol) of AIBN that was dissolved into 0.5 mL of distilled THF. After this mixture was stirred for 15 min at 600 rpm to facilitate the sorption of AIBN by the particles, the flask was immersed into an oil bath that was preheated to 90 °C. A mixture of HEA-Cl (0.40 g, 1.9 mmol), EGDMA (40 μL, 0.21 μmol), and 0.67 g MMA (6.7 mmol) were added dropwise using a syringe pump at a flow rate of 2.03 mL/h. After monomer addition, the heating at 90 °C was continued for 4 h to complete shell growth.

The CS particles were settled by centrifugation at 16 000 rpm (28 930 *g*) for 20 min. The supernatant was then decanted, and the particles were redispersed by vigorous stirring into 100 mL of deionized water. The centrifugation and supernatant removal procedure then was repeated. The precipitate was dried under vacuum to give 2.0 g of the product at 75% yield.

Core−Shell−Corona Particles. CSC particles were prepared by growing PHEA chains from the CS particle surfaces. Three types of CSC particles were prepared using the HEA:HEA-Cl molar feed ratios of 220:1, 430:1, and 1500:1. The resultant particles were denoted as CSC-1, CSC-2, and CSC-3, respectively.

To prepare CSC-2, 13.6 mg of the CS particles containing 8.9×10^{-3} mmol of HEA-Cl were dispersed into 5.0 mL of water/methanol (at v/v = 1/1) in a 50-mL Schlenk flask. A combination of 23.0 mg (0.160 mmol) of CuBr, 2.3 mg (0.010 mmol) of $CuBr_2$, and 64.5 mg (0.28 mmol) of Me_6TREN was added to the dispersion. Methyl 2-chloropropionate (0.9 mg, 8.5×10^{-3} mmol) in 0.45 mL of methanol/water (at v/v = 1/1) and HEA (0.7456 g, 6.42 mmol) also were added. The mixture was degassed thrice, using a cycle consisting of sample freezing, pumping, thawing, and N_2 backfilling. This mixture was then stirred for 30 min at room temperature, and the flask was immersed into an oil bath that was preheated to 75 °C. After 10 h of heating, followed by cooling to room temperature, the mixture was diluted by 5.0 mL of a water/methanol mixture (v/v = 1/1) and centrifuged at 3800 rpm (2850 *g*) for 10 min to settle the particles. The particles were redispersed into water, and the resultant solution was centrifuged to resettle the particles. This rinsing step was repeated thrice before the redispersed particles were dialyzed against water in a tube with a cutoff molecular weight of 12000−14000 g/mol to remove small-molecule impurities. Finally, the particles were settled by centrifugation and dried under vacuum to yield a white powder. The particle yield, which is defined as the ratio between the mass of the obtained CSC-2 particles and the total mass of the fed CS particles and HEA monomer, was determined gravimetrically to be 76%.

The supernatant of the reaction mixture after settling the CSC particles contained the free polymer chains that were initiated by methyl 2-chloropropionate. The original supernatant and those from the later CSC particle rinsing steps were combined, condensed by a rotary evaporator, and then passed through a silica gel column to remove the catalysts. The resultant PHEA solution was concentrated for size exclusion chromatography (SEC) analysis.

SEC Analysis. The PHEA samples were characterized by an SEC system that was operated at 70 °C. The columns consisted of AM GPC Gel (1000 Å, 10 000 Å, and 100 000 Å), and a Water 2410 differential refractometer was used as the detector. The system was calibrated by monodisperse polystyrene standards. Dimethylformamide (DMF) at a flow rate of 0.90 mL/min was used as the eluant.

CSC Particle Fluorination. The CSC particles were fluorinated by reacting the hydroxyl groups of PHEA chains with perfluorononanoyl chloride. To fluorinate the CSC-3 particles, the particles were dissolved

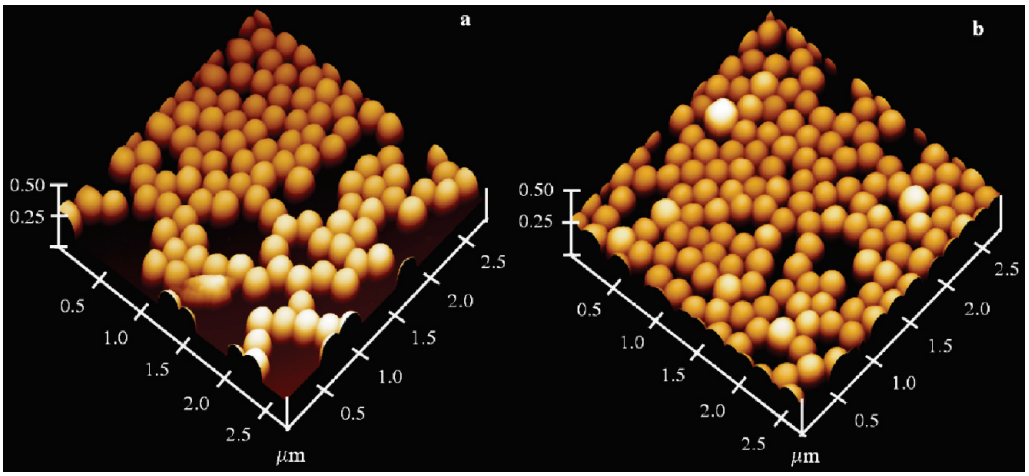

Figure 1. AFM 3-D topography images of (a) C particles and (b) CS particles that were prepared by emulsion polymerization and sprayed on mica surfaces.

in dry pyridine at a concentration of 5.0 mg/mL. Perfluorononanoyl chloride (25 mg) was then slowly added as a neat liquid into 1.0 mL of the particle solution with stirring. After the addition, the system was stirred at room temperature for 18 h. The precipitate was then collected and washed with pyridine and methanol to remove byproducts before it was dried under vacuum to yield 15 mg of product CSC-3F. The CSC-1 and CSC-2 were fluorinated analogously to yield CSC-1F and CSC-2F.

The ^{1}H NMR spectra of the fluorinated particles were recorded on a Bruker Avance 500 MHz spectrometer. The solvent used consisted of a α,α,α-trifluorotoluene/deuterated chloroform mixture at v/v = 3/1.

Physically-Deposited Particulate Coatings. The fluorinated particles were dispersed into α,α,α-trifluorotoluene or trifluorotoluene and the CSC particles were dispersed in methanol at 3.0 mg/mL, respectively. The fluorinated particle solution was then cast onto glass slides to yield physically deposited coatings by three methods. In Method 1, coatings were obtained by spin coating a drop of the solution onto a glass slide at 3000 rpm. Method 2 involved dispensing several drops of the solution onto a glass slide and subsequently spreading them with a glass rod. In Method 3, a glass slide was tilted at ∼45° and several drops of the solution were then applied. The CSC particle coatings were prepared by Method 1. In every case, at least 4 h was allowed for the solvent to evaporate at room temperature before contact angle measurements.

Covalently Attached Superhydrophobic Coatings. Part A and Part B of the Varian Torr Seal epoxy glue were mixed at a volume ratio of 2:1. Approximately 0.1 mL of this mixture was dispensed onto a 0.7 cm × 0.7 cm glass plate, which was subsequently spun at 10 000 rpm for 1 min. The resultant film had a thickness of ∼0.5 mm and was heated in a 60 °C oven for 1 h to partially cure the glue. On this glue surface was then aero-sprayed, using a home-built device,[42] 0.2 mL of a 2 mg/mL CSC-2F solution in trifluorotoluene. The composite film was heated at 70 °C for 1 h and cooled to room temperature before liquid contact angle measurements.

Fluorinated Particles on PCEMA Film. In a control experiment, a composite film was prepared by depositing the CSC-2F particles on a film of a photo-cross-linkable polymer, poly(2-cinnamoyloxyethyl methacrylate) (or PCEMA), which had 100 repeat units. This first invoked spin-coating, at 300 rpm for 1 min, a 0.2 g/mL PCEMA solution in chloroform onto a 0.7 cm × 0.7 cm glass plate and drying the resultant film at room temperature for 3 h. The film was then irradiated for 15 min by a focused beam that had passed through a 270-nm cutoff filter from a 500-W mercury lamp in an Oriel 6140 lamp housing powered by an Oriel 6128 power supply. The CEMA double-bond conversion, determined from the absorbance decrease at 274 nm, was 48%.[43] The CSC-2F solution in trifluorotoluene was then aero-sprayed onto the partially cross-linked PCEMA film. The composite film with polymeric particles was further irradiated for 2 h to reach a final CEMA double bond conversion of ∼90%.

Particle Extraction from the Composite Films. CSC-2F/epoxy and CSC-2F/PCEMA composite films were stirred with ∼20 mL of trifluorotoluene at 180 rpm for 16 h. The glass-plate-backed films were then dried at 100 °C for 30 min.

Dynamic Light Scattering Measurements. Dynamic light scattering (DLS) measurements were carried out at 21 °C using a Brookhaven BI-200 SM instrument that was equipped with a BI-9000AT digital correlator and a He−Ne laser (632.8 nm). The samples in light scattering cells were centrifuged at 2500 rpm (1250 *g*) for 25 min before they were inserted gently into the DLS sample holder for measurements at 90°. The data were analyzed using the Cumulant method to yield the hydrodynamic diameter d_h and polydispersity index K_1^2/K_2.[44]

Contact Angle Measurements. The contact angles of the surfaces were measured using a KRUSS K12 tensiometer that was interfaced with image-capturing software. Samples were injected as 5-μL liquid drops. Measurements were performed at room temperature, using two probe liquids, including water (Milli-Q, with a surface tension of 72.8 mN/m at 20 °C) and diiodomethane (>99%, Sigma−Aldrich, with a surface tension of 50.8 mN/m at 20 °C).[45,46]

X-ray Photoelectron Spectroscopy. X-ray photoelectron spectroscopy (XPS) measurements were taken using a Thermo Instruments Microlab 310F surface analysis system (Hastings, U.K.) under ultrahigh vacuum conditions. The Mg Kα X-ray (1486.6 eV) source was operated at a 15 kV anode potential with a 20 mA emission current. Scans were acquired in the Fixed Analyzer Transmission (FAT) mode, with a pass energy of 20 eV and a surface/detector takeoff angle of 75°. All spectra were calibrated to the C 1s line at 285.0 eV, and minor charging effects were observed, which produced a binding energy increase between 1.0 eV and 2.0 eV.

Transmission Electron Microscopy Measurements. For staining the CS particles, 10.0 mg of the CS particles, containing 6.5 × 10^{-3} mmol of HEA-Cl, was initially dissolved into 1.0 mL of methanol and then 2.0 mg of silver trifluoromethanesulfonate (7.8 × 10^{-3} mmol) was added. The solution was stirred at 50 °C for 2 and 4 d, before it was cooled and sprayed onto the carbon-coated copper transmission electron microscopy (TEM) grid. TEM images were obtained using a Hitachi-7000 instrument operated at 75 kV.

Table 1. Characteristics of the Spheres at Different Stages

	DLS[a]		AFM	
sample	d_h (nm)	K_1^2/K_2	d_{AFM} (nm)	h_{AFM} (nm)
C	257 ± 5	0.001−0.024	246 ± 12	173 ± 9
CS	323 ± 5	0.013−0.015	287 ± 15	199 ± 11
CSC-1	360 ± 6	0.003−0.007	344 ± 17	225 ± 14
CSC-2	449 ± 3	0.005−0.008	383 ± 21	248 ± 15
CSC-2F	473 ± 9	0.004−0.007	432 ± 16	257 ± 14
CSC-3	606 ± 8	0.005−0.014	572 ± 37	403 ± 24
CSC-3F	697 ± 17	0.005−0.013	644 ± 44	421 ± 52

[a] DLS analyses of the fluorinated particles were done in α,α,α-trifluorotoluene, and those of all other particles were done in water.

Atomic Force Microscopy (AFM). Specimens were prepared by spraying solution samples onto freshly cleaved mica surfaces and dried under vacuum. All samples were analyzed by atomic force microscopy (AFM) in the tapping mode, using a Veeco multimode instrument equipped with a Nanoscope IIIa controller.

III. RESULTS AND DISCUSSION

Core Particles. As mentioned in the Introduction, the core particles were prepared by the surfactant-free emulsion polymerization of MMA and EGDMA. This technique is well-established and should yield uniform spheres.[47,48] Our success in using this technique was confirmed by our AFM and DLS studies of the particles.

Figure 1a shows an AFM topography image of the core particles denoted as C. The sample consisted of uniform spheres. A quantitative analysis yielded an AFM diameter (d_{AFM}) and height (h_{AFM}) of 246 ± 12 and 173 ± 9 nm, respectively, where the numbers after the ± signs denote the standard deviation in the dimension readings. Thus, the relative deviations of the d_{AFM} and h_{AFM} values were <5% and in agreement with those expected of particles prepared from emulsion polymerization.[49] The h_{AFM} value was smaller than the corresponding d_{AFM} value, because the spheres should flatten somewhat when they plummeted, together with the spraying solvent, on a substrate during specimen preparation. Also, d_{AFM} contained a contribution from the finite size of the AFM tip.

The diameter (d_h) of the C particles probed by DLS was 257 nm with a polydispersity index (K_1^2/K_2) of 0.001−0.024 (see Table 1). The d_h value was slightly larger than d_{AFM}, because d_h and d_{AFM} were the z-average and number-average diameters, respectively. Furthermore, d_h was measured in a solvated state and d_{AFM} was measured in the dry state. The polydispersity index reading varied from run to run, because it was difficult to remove trace amounts of dust particles from the system. If the dust particles entered the scattering volume during data acquisition, the calculated K_1^2/K_2 value increased for that run. Despite this, all recorded K_1^2/K_2 values were low, confirming the narrow distribution of the particles.

Core−Shell Particles. The core−shell (CS) particles were prepared by seeded emulsion polymerization. Figure 1b shows an AFM topography image of a CS sample, which was derived from C. The AFM image clearly revealed that the particles were uniformly sized and had a narrow size distribution. The d_{AFM} and h_{AFM} values, as well as other size characteristics of this sample, are listed in Table 1. The low DLS K_1^2/K_2 value attests to the low polydispersity of the particles. Compared to the d_h, d_{AFM}, and h_{AFM} values of the C particles, those of the CS particles increased by 25%, 17%, and 15%, respectively.

Seeded emulsion polymerization, if done properly, should impart particles that possess low polydispersities. Provided that the monomer is completely consumed and no new nuclei are formed during shell formation, the diameters d_f and d_c of the CS and C particles are related by[49]

$$d_f = (V_f/V_c)^{1/3} d_c \quad (1)$$

where V_c and V_f are the volumes of the core and the final particles, respectively. Neglecting the density difference between the shell and core polymers, we calculated V_c and V_f from the mass of the core particles and that of the secondary monomers that were used to prepare the shell. Inserting this information into eq 1 yielded a d_f/d_c value of 1.17. Thus, the diameter of the CS particles should have increased by ∼17%, relative to that of the C particles. This value compares well with the d_{AFM} and h_{AFM} increases of 17% and 15% for CS relative to C, but was smaller than the 25% increase for the CS d_h value.

Several factors might have contributed to the larger d_h value increase. First, there might have been some error in the measured d_h values. Second, the EGDMA molar feed ratio was 2.2% for the shell but 4.0% for the core. Third, HEA-Cl should be more polar than the other monomers. Because of the latter two reasons, the shell might be more swollen in water than the core.

Seeded emulsion polymerization does not necessarily produce CS particles that have a shell made of monomers added during the second polymerization stage. Depending on the monomers used and their addition mode, the resultant particles can have morphologies other than the desired morphology.[50−52] Despite this, one can target the core−shell structure by controlling either the thermodynamics and/or the kinetics of a polymerization system. If the newly formed polymer prefers the water/polymer interface, the CS particle will form most likely as a thermodynamic product. Even if the newly formed polymer has a higher water/polymer interfacial tension than that of the precursor polymer, it is still possible to prepare the targeted CS particles as a kinetic product.

To prepare the targeted CS particles as a kinetic product, one can, for example, add the second batch of monomer(s) into a polymerizing system dropwise, or perform the seeded emulsion polymerization in a semibatch mode under monomer-starved conditions. The slow addition of the new monomer(s) serves two purposes. First, it helps minimize new nucleation. Second, it eliminates core particle swelling by the secondary monomer(s) and avoids their polymerization inside the core particles. The secondary monomer(s) should polymerize preferentially at the water/particle interface, as a result of diffusion through the aqueous phase and incorporation into the particles. To ensure that the newly formed polymer remains trapped in the shell layer, even if this is not its favored position, one can prepare polymers that either have high glass-transition temperatures or are cross-linked.

The cross-linker EGDMA was added during the formation of both the cores and the shells of our particles. Also, the secondary monomers HEA-Cl, MMA, and EGDMA were slowly pumped into the polymerization flask. Furthermore, HEA-Cl should be more polar than MMA and EDGMA. Thus, we expected shell formation from our secondary monomers.

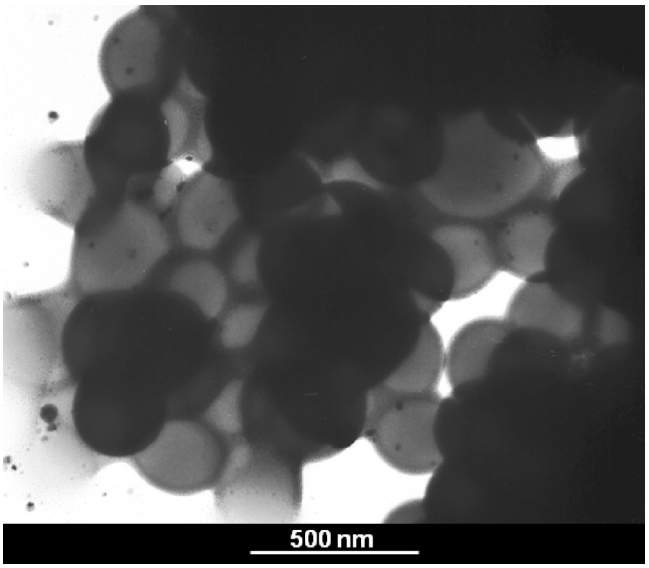

Figure 2. TEM image of CS particles stained with CF_3SO_3Ag and sprayed from methanol. HEA-Cl in the outer layer reacted with CF_3SO_3Ag to produce AgCl.

We confirmed the anticipation by transmission electron microscopy (TEM). This relied on developing an effective method for staining the HEA-Cl groups. Our hypothesis was that the CS particles should swell in methanol and, thus, silver triflate should be able to diffuse into the particles if enough time and a driving force were provided for this process. The labile chloride group of HEA-Cl should react with silver triflate and water to produce AgCl at locations where HEA-Cl was present:[53]

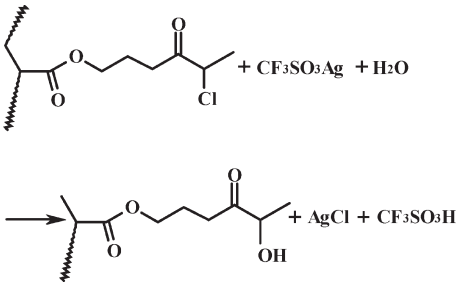

With both Ag and Cl being heavy atoms, AgCl should scatter electrons more effectively than the elements found in the organic polymers. Thus, locations that originally contained HEA-Cl should appear darker under a microscope.

Figure 2 shows a TEM image of a CS sample thus treated. After CF_3SO_3Ag staining, the particles' outer rim appeared dark. It is plausible that the dark rim had resulted from CF_3SO_3Ag that entered the particles by pure diffusion. However, we ruled out this possibility for the following reasons. First, the molar ratio used between HEA-Cl and CF_3SO_3Ag was close to 1/1. If not for the reaction between HEA-Cl and CF_3SO_3Ag, no particular driving force existed for CF_3SO_3Ag to partition into the particles. Second, the thickness of this dark layer did not increase by prolonging the equilibration time between the CS particles and the silver triflate solution from 2 d to 4 d. This contradicted what was expected of the pure silver triflate diffusion mechanism. Third, the thickness of this dark layer was 28 ± 3 nm, which agreed with the shell thickness of 33 nm calculated from the d_h values for the C and CS particles.

In addition to the above experiment, we have also performed the ^1H NMR analysis of the CS particles in pyridine-d_5. The signals for HEA-Cl at 1.7 and 4.5 ppm were clearly observed for the particles, confirming the incorporation of the HEA-Cl into the particles.

Core−Shell−Corona Particles. The coronal PHEA chains were grown via ATRP from the CS particle surfaces in water/methanol at v/v = 1/1. Controlled solution ATRP of HEA was first reported by Matyjaszewski and co-workers.[54] Even when done from the surfaces of latex particles[36] and silica particles,[55] HEA ATRP was also shown to be controlled. Based on these prior results, we anticipated the controlled ATRP of HEA in our case as well.

Figure 3 shows AFM topography images of three batches of CSC particles. The CSC-1, CSC-2, and CSC-3 particles were all derived from the same CS particles, but were prepared using the different HEA to HEA-Cl molar ratios ($n_{HEA}/n_{HEA\text{-}Cl}$) of 220/1, 430/1, and 1500/1, respectively. Evidently, the AFM images suggest that the CSC particle size increased as $n_{HEA}/n_{HEA\text{-}Cl}$ increased. This has also been confirmed by the increases in the d_h value (see Table 1). More interestingly, the shape of the particles changed from CSC-1 spheres, to CSC-2 bumpy spheres, and then to CSC-3 spheres bearing fused surface "lobes".

The particle size expanded with increasing $n_{HEA}/n_{HEA\text{-}Cl}$, because the HEA ATRP reaction was controlled and the surface PHEA chain lengthened with increasing $n_{HEA}/n_{HEA\text{-}Cl}$. To shed light on the properties of the PHEA chains prepared during the corona growth, we mixed some free initiator, methyl 2-chloropropinate, with the CS particles before the polymerization. Initiation of HEA polymerization by methyl 2-chloropropinate resulted in free PHEA chains in the solvent phase. These free PHEA chains were then analyzed by SEC against monodisperse PS standards, and the results are given in Table 2. The SEC M_n values of the free PHEA increased with $n_{HEA}/n_{HEA\text{-}Cl}$, as anticipated. The low M_w/M_n value of 1.15 for the free PHEA chains at $n_{HEA}/n_{HEA\text{-}Cl}$ = 220 and the reasonably low M_w/M_n value of 1.43 at $n_{HEA}/n_{HEA\text{-}Cl}$ = 1500 suggested that the HEA free-radical polymerization was controlled.

The M_n values in Table 2 did not grow linearly with $n^{HEA}/n_{HEA\text{-}Cl}$, probably for several reasons. First, we did not know the fraction of HEA-Cl units that initiated HEA polymerization. Second, the characteristics of the free PHEA chains may have differed from those grafted onto the CS particles. Third, we did not determine the exact HEA conversions for the different polymerizations. Fourth, the SEC M_n values were not absolute, but were calculated based on PS standards. We did not strive to resolve these issues, because this research's primary objective was to prepare amphiphobic spheres rather than spheres with a precisely controlled coronal thickness.

The fraction of HEA-Cl units that did initiate HEA polymerization should change significantly, depending on the solvent(s) used for ATRP. Brooks and co-workers[36] grew PHEA and poly(*N*,*N*-dimethylaminoethyl methacrylate) chains from poly[styrene-*co*-(HEA-Cl)] latex particle surfaces in water, which swelled the core particles insignificantly. Their meticulous work demonstrated that only HEA-Cl units that were in the outer ~1.5 nm surface layer initiated HEA polymerization. Stover and co-workers[31] grew polymer chains from cross-linked polymer particle surfaces in THF, which solvated the core, and suggested that chains initiated from sites that were deep inside the particles.

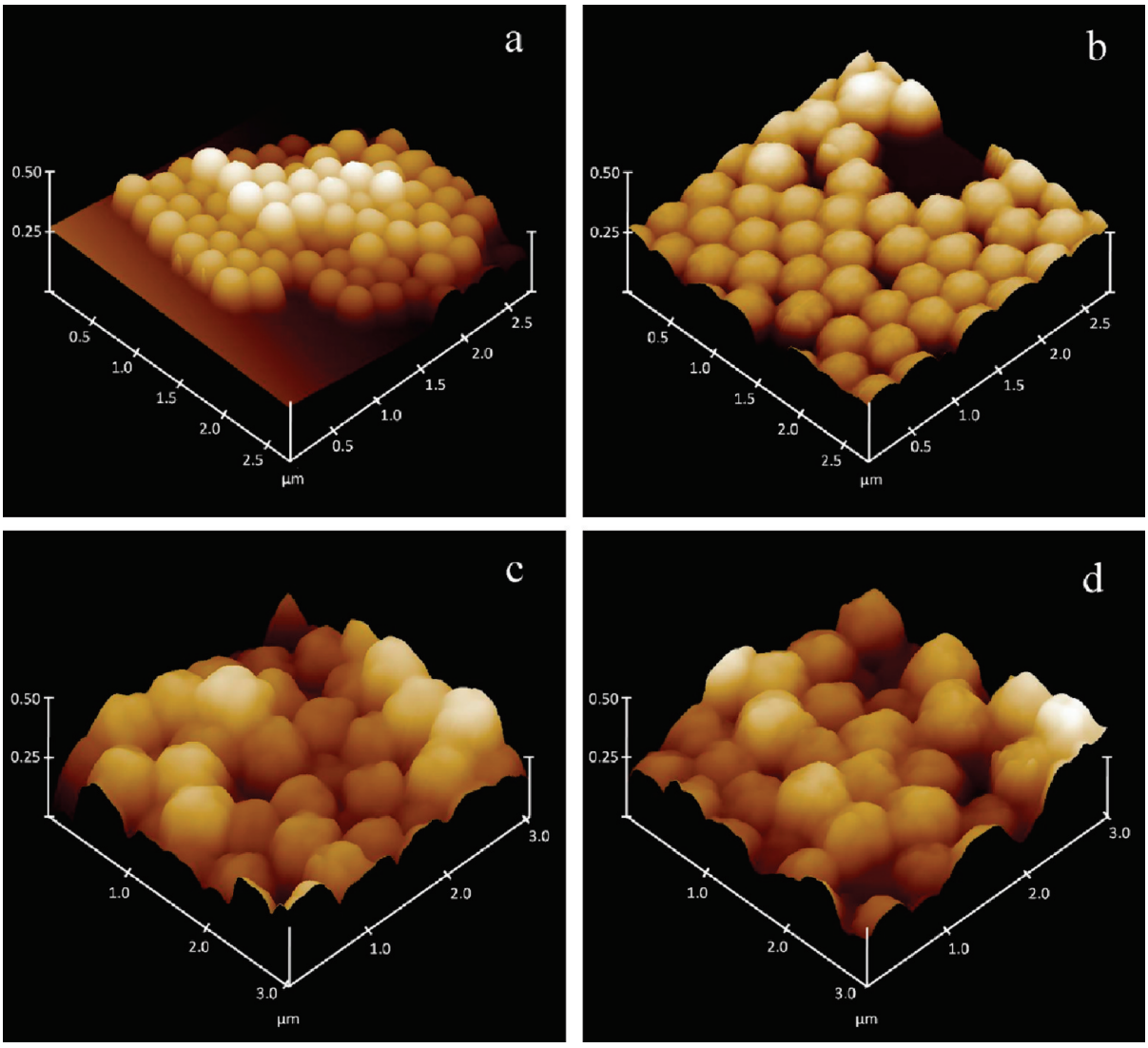

Figure 3. AFM 3-D topography images of (a) CSC-1, (b) CSC-2, (c) CSC-3, and (d) CSC-3F particles that were sprayed on mica surfaces.

Table 2. SEC Characteristics of the Linear PHEA Chains Prepared Together with the CSC Particles

sample	$n_{HEA}/n_{HEA\text{-}Cl}$	SEC M_n (g/mol)	SEC M_w/M_n
CSC-1	220	2.1×10^4	1.15
CSC-2	430	5.6×10^4	1.30
CSC-3	1500	9.1×10^4	1.43

Our ATRP was performed in water/methanol, which is a solvent mixture that swelled the CS particles only slightly. Thus, we suspect that mainly the surface HEA-Cl units initiated polymerization.

Past studies demonstrated that the free polymer chains grown from added small-molecule initiators had molecular weights identical to those of the surface-grafted chains. These previous studies utilized particles such as silica, gold, and iron oxides, which had impermeable cores.[56] The latex particles used in this study could be permeated by ligands, monomer, and catalyst. Therefore, the M_n and M_w/M_n values reported in Table 2 may differ from those of the grafted polymer chains. Despite this, the observed trends for M_n and M_w/M_n should be similar for the free and grafted chains.

The formation of bumps and lobes on the CSC-2 and CSC-3 particle surfaces was likely due to both kinetic and thermodynamic factors. We observed that the bumps were larger when the CSC-2 particles were sprayed from the more-volatile solvent methanol than from water. This suggests that kinetics were a contributing factor to the final bump size. The bumps never disappeared despite annealing (for 2 days) the sprayed samples at 90 °C, which was above the glass-transition temperature of 10 °C for PHEA.[57] This suggests that these bumps were thermodynamically stable. Similar surface structures have been observed for long chains grown on other types of polymer particles.[31]

We suspect that the ultrahigh density of the grafted chains close to the corona/shell interface and the polydispersity of the grafted chains are the thermodynamic causes for surface bump or lobe formation. Past studies[56] have demonstrated that surface-initiated ATRP can produce polymer brushes with grafting densities approaching 1 chain/nm^2. Because of this crowdedness, and thus the strong interchain repulsion, these chains are almost fully stretched in their solvated state. Even after drying, the chains

dx.doi.org/10.1021/cm103673j |*Chem. Mater.* 2011, 23, 2810–2820

Scheme 2. Schematic Illustration of Bump (Top) and Lobe (Bottom) Formation from Less-Polydisperse and More-Polydisperse Surface Chains

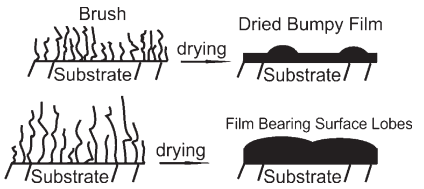

do not collapse significantly vertically, and the thickness of the resultant films can reach 40% of the contour length of the fully stretched chains.[56] It is instructive to imagine that the grafted chains are polydisperse. The greater the distance from the shell/corona interface, the fewer the number of remaining chains. Furthermore, the surface area available to accommodate the longer or remaining chains increases. Therefore, the chains become less crowded as the radius r increases. Upon drying such a polymer layer, the long chains could not retract much along the radial direction, because of the high segmental density close to core particle surface. Therefore, the less-crowded terminal ends of the long chains aggregate to form the towering bumps or lobes.

The bumps and lobes are both protruding structures. As illustrated in Scheme 2, the bases of the lobes overlap with each other, and the bumps are better-resolved lobes. The lobes are formed from longer and more-polydisperse surface chains.

Table 1 reveals that the polydispersity of the grafted PHEA chains increased from CSC-1 to CSC-2 and CSC-3 particles. The polydispersity criterion explains why no obvious bumps were seen on the CSC-1 particles, but were seen on the CSC-2 and CSC-3 particles.

Corona Fluorination. The coronal PHEA chains were fluorinated by reacting the PHEA hydroxyl groups with perfluorononanoyl chloride in pyridine:

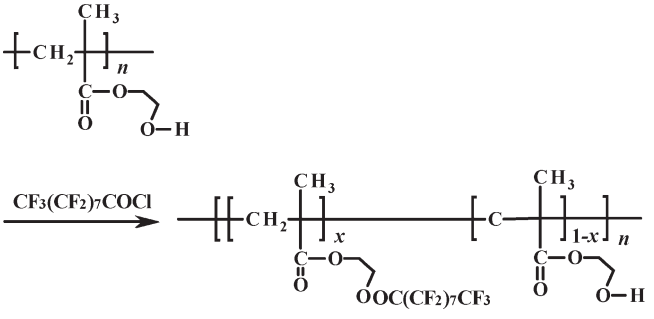

Figure 4 shows a ^{1}H NMR spectrum of the fluorinated CSC-3 or CSC-3F particles in $CDCl_3$ and trifluorotoluene. After fluorination, the positions of the ethylene protons of the hydroxyl ethyl groups shifted downfield. A comparison of the integrated areas of peaks c and d of the fluorinated units and those of peaks a and b of HEA units revealed that 80% of the PHEA hydroxyl groups of CSC-3 were fluorinated.

We analyzed the CSC-1F and CSC-2F spheres similarly and determined that the degrees of fluorination for these spheres were the same, within experimental errors, at 80%. The 80% fluorination determined by ^{1}H NMR should be taken with caution. The PHEA segments close to the shell/corona interface may be so dense that their segmental tumbling motion may be

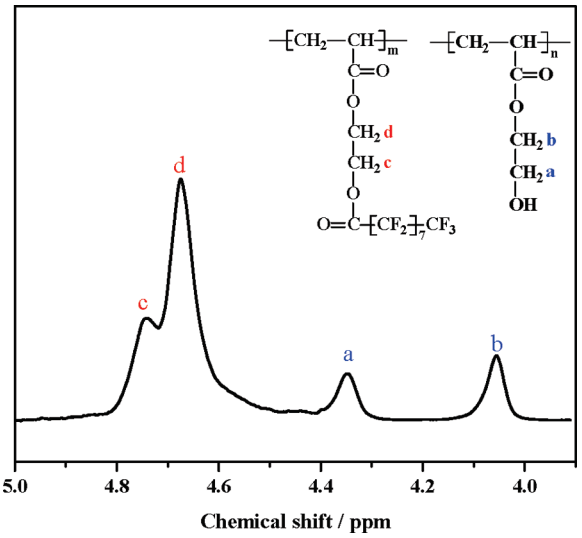

Figure 4. ^{1}H NMR spectrum CSC-3F particles in trifluorotoluene and $CDCl_3$ at v/v = 3/1.

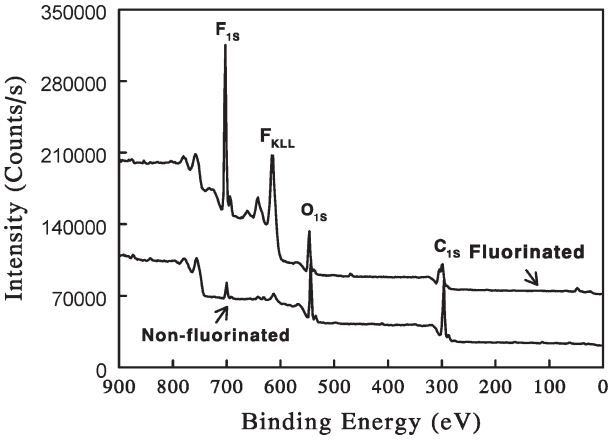

Figure 5. XPS spectra of the CSC-3 particles before fluorination (bottom spectrum) and of the CSC-3F particles obtained after fluorination (top spectrum).

restricted. Thus, ^{1}H NMR might not be able to detect these segments. The measured 80% degree of fluorination might be for those segments that were closer to the outer edge of the corona and not for all PHEA hydroxyl groups.

The successful fluorination was also confirmed by an X-ray photoelectron spectroscopy (XPS) study. Figure 5 compares the XPS spectra of CSC-3 and CSC-3F. Before fluorination, the O 1s and C 1s peaks were dominant. This was in agreement with the fact that PHEA was composed mainly of carbon, hydrogen, and oxygen and the H 1s peak was not detectable. After fluorination, one F 1s peak and a group of fluorine Auger peaks (F_{KLL}) appeared in the spectrum of CSC-3F.[58]

Figure 3d shows an AFM topography image of CSC-3F spheres. The particle morphology did not change with fluorination. The data in Table 1 clearly show that the size of the CSC particles increased after fluorination, because of the increased mass of the corona.

Amphiphobicity of the Fluorinated Particles. The successful corona fluorination was further confirmed by liquid contact

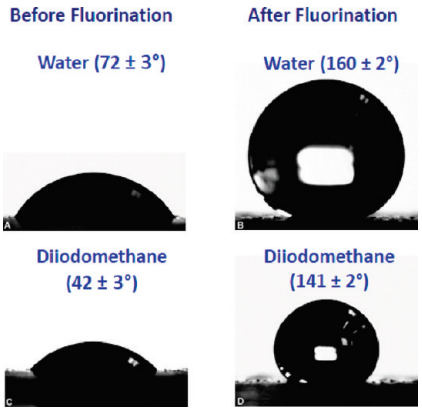

Figure 6. Photographs of (A and B) water and (C and D) diiodomethane droplets on films made of CSC-3 particles (A and C) and CSC-3F particles (B and D).

Table 3. Advancing, Static, and Receding Contact Angles (θ_A, θ_S, and θ_R, Respectively) of Water and Diiodomethane Droplets on Coatings Made from Different Spheres

	Water			Diiodomethane		
coating sample	θ_A (deg)	θ_S (deg)	θ_R (deg)	θ_A (deg)	θ_S (deg)	θ_R (deg)
CSC-3	78 ± 2	72 ± 2	59 ± 2	47 ± 2	42 ± 2	37 ± 2
CSC-1F	157 ± 2	152 ± 2	151 ± 2	135 ± 2	129 ± 2	122 ± 2
CSC-2F	161 ± 2	157 ± 2	154 ± 2	139 ± 2	135 ± 2	126 ± 2
CSC-3F	165 ± 2	160 ± 2	157 ± 2	144 ± 2	141 ± 2	135 ± 2

angle measurements on coatings made from the fluorinated and nonfluorinated CSC particles. Figure 6 compares photographs taken of H_2O and CH_2I_2 droplets sitting on coatings that were prepared by spin-coating CSC-3 and CSC-3F solutions on glass plates. The static H_2O and CH_2I_2 contact angles (θ_S) increased from 72° ± 3° and 42° ± 3° on the CSC-3 coatings to 160° ± 2° and 141° ± 2° on CSC-3F coatings. This agreed with the reduced surface energy of the fluorinated particles.

Table 3 further lists the advancing and receding contact angles (θ_A and θ_R, respectively) for these droplets. The difference between the θ_A and θ_R values and, thus, the hysteresis were small for each liquid. Furthermore, all contact angles including θ_A, θ_S, and θ_R were larger than 150° for water droplets. Therefore, the surfaces of CSC-3F particles were superhydrophobic. The θ_A, θ_S, and θ_R values also were large for CH_2I_2 droplets. This suggests that the CSC-3F coatings were also oil-repellent, and thus they were amphiphobic.

Particulate coatings were prepared also from the CSC-1F and CSC-2F, and the measured H_2O and CH_2I_2 contact angles were also included in Table 3. Regardless of the particle type, the coatings of all the fluorinated particles were superhydrophobic.

The water contact angle on a flat fluorinated surface is ~120°.[59] The contact angles were all larger than 150° on coatings prepared from our particles, because all of our coatings were rough. The roughness of our coatings was attributable to two reasons. First, a closely packed rugged particle array rather than a continuous film was formed from our particles. This arose from the facts that both the core and the shell of the particles were cross-linked and were not deformable and that the ultradense coronal chains of different particles did not interpenetrate extensively with each other.[60,61] Second, bumps and lobes were formed by the surface chains of the fluorinated CSC particles. This multilevel roughness was clearly seen in Figures 3c and 3d, which showed AFM images of CSC-3 and CSC-3F coatings.

Table 3 further reveals that the θ_A, θ_S, and θ_R values of both liquids increased from the CSC-1F coatings to the CSC-2F and CSC-3F coatings. This increasing trend was not an artifact of the coating preparation protocol, because three physical deposition methods, as described in the Experimental Section, were used to prepare the particulate coatings and the θ_A, θ_S, or θ_R values of a particular sample changed little with the coating preparation methods. Thus, this θ variation trend most likely had its roots in the packing and morphology variation of the particles.

Since the observed contact angle hysteresis was small on all particulate coatings,[62] the liquid droplets should have existed in the metastable Cassie state, meaning that the droplets were suspended above the surface by the fluorinated solid protrusions and air pockets were trapped between the droplet and the valleys.[11,14,19] In this state, the observed contact angle on a rough surface (θ_o) and that on a flat surface (θ_f) were related by

$$\cos\theta_o = f(1 + \cos\theta_f) - 1 \qquad (2)$$

Here, f is the ratio between the droplet/solid contact area and the total contact area made by the droplet with the solid protrusions and trapped air.

The θ_o value increased from CSC-1F to CSC-2F and CSC-3F coatings because f decreased in this order. This should not have been a direct consequence of the particle size increase, because f should not change with particle size if the particles were sufficiently large and were packed regularly to yield a uniform even top layer. This has been experimentally verified by Tsai et al.[63] for even layers of alkylated silica particles that had diameters of 0.5, 1.0, and 1.5 μm and were deposited using the Langmuir−Blodgett method.

While particle size changes do not directly affect the observed θ values, they do change the spatial packing of the particles in a coating and, therefore, indirectly affect the θ values observed. However, a theoretical formulation of this effect is dependent on the particle packing model and is difficult. Fortunately, some general trends seem to exist among the literature results. For example, Cao et al. dispersed silica of different sizes in a polymer binder to yield composite coatings.[64] Water contact angles on these coatings initially increased with silica size, maximized at the silica size of ~100 nm, and then decreased with further increase in silica size. Xiu et al.[65] dispersed 200-nm and 5-μm Teflon particles inside silicone Sylgard to prepare composite coatings and found that the water contact angles were ~30° higher on coatings prepared from the smaller Teflon particles. Our fluorinated particles had sizes in the range of 350−650 nm. If the prior results were of any guidance value, increasing the size of the particles from CSC-1F to CSC-2F and CSC-3F should have also changed the spatial packing of the particles, such that the liquid contact angles should have decreased.

Therefore, the surface bumps and lobes of the CSC-2F and CSC-3F particles were most probably responsible for the observed θ variation trend. This should not be surprising because bumpy spheres, possessing roughness at two length scales, have been shown by many different groups to perform better than smooth spheres in the creation of superamphiphobic surfaces.[58,59,62,63,66−68] The use of multilength scale roughness

is also how nature creates superhydrophobic surfaces from simple hydrocarbons or waxes, which are not intrinsically as hydrophobic as fluorinated polymers.[8,10]

Covalently-Bonded Particulate Coating. The particulate coatings that we have discussed so far were physically deposited on glass plates and the adhesion forces between the substrate and particles and among the particles were weak. To prepare covalently bonded coatings from CSC-2F, we first spin-coated an epoxy glue mixture consisting the glycidyl part and the multiamine part onto glass plates. After this glue was partially cured, CSC-2F particles in trifluorotoluene were then aero-sprayed onto the glue. The composite coatings were then further cured, so that the hydroxyl groups in the CSC-2F corona could react with the residual glycidyl units in the epoxy glue.

The composite coatings mentioned above should be layered with the CSC-2F particles at the top. Not surprisingly, the H_2O and CH_2I_2 contact angles, shown in Table 4, on these coatings were almost identical to those reported for the physically deposited CSC-2F coatings. A much more interesting observation was that the liquid contact angles, as given in Table 4, changed negligibly after these coatings were stirred for 16 h with trifluorotoluene, which should have extracted CSC-2F particles that were not covalently attached to a substrate and solubilized a physically deposited CSC-2F coating.

To show that this improved adhesion between the CSC-2F particles and the epoxy matrix was not due to the physical entrapment of the particles by cross-linked polymer chains, we performed a control experiment. In it, a layer of PCEMA, which could undergo photo-cross-linking,[42] was used to replace the epoxy layer. Analogously, the CSC-2F particles were aero-sprayed onto a partially cross-linked PCEMA layer. This was followed by further irradiation of the composite coating to cross-link the PCEMA layer more. The liquid contact angles on this coating were the same, within experimental errors, as those on the CSC-2F/epoxy composite coatings. After particle extraction by triflourotoluene, the contact angles decreased drastically. These suggested the removal of the particles from the PCEMA surface and inability of the cross-linked PCEMA chains or the cross-linked epoxy matrix to physically trap CSC-2F particles. Therefore, the CSC-2F particles were retained by the epoxy glue, because the CSC-2F coronal hydroxyl groups had reacted with the glycidyl groups of the epoxy glue.

Figure 7 compares the AFM topography images of the CSC-2F/epoxy glue and CSC-2F/PCEMA composite coatings after CSC-2F particle extraction by trifluorotoluene. Evidently, a CSC-2F layer was retained by the epoxy glue after the trifluorotoluene extraction step. On the other hand, many holes were seen in the trifluorotoluene-extracted CSC-2F/PCEMA layer, confirming the removal of the CSC-2F particles in this case.

Table 4. Advancing, Static, and Receding Contact Angles of H_2O and CH_2I_2 on Composite Coatings That Were Made of CSC-2F and Polymer Resin before and after Particle Extraction by Trifluorotoluene

	Water			Diiodomethane		
resin/extraction	θ_A (deg)	θ_S (deg)	θ_R (deg)	θ_A (deg)	θ_S (deg)	θ_R (deg)
epoxy/before	162 ± 2	161 ± 2	154 ± 2	140 ± 2	138 ± 2	127 ± 2
epoxy/after	159 ± 2	156 ± 2	153 ± 2	138 ± 2	134 ± 2	126 ± 2
PCEMA/before	161 ± 2	158 ± 2	155 ± 2	139 ± 2	136 ± 2	124 ± 2
PCEMA/after		104 ± 2			83 ± 2	

IV. CONCLUSIONS

Emulsion polymerization, seeded emulsion polymerization, and ATRP were used in sequence to prepare CSC particles. Following our design, the HEA-Cl units were localized in the shell layer of the CS particles derived from the seeded emulsion polymerization. This was confirmed by a TEM study that utilized a novel method for staining the HEA-Cl units. The corona was prepared from HEA-Cl-initiated ATRP of HEA. The corona thickness increased as the feed molar ratio for HEA and HEA-Cl increased, suggesting that the polymerization was controlled. Particles with long coronal PHEA chains bore interesting surface bumps or lobes. Eighty percent of the PHEA hydroxyl groups were shown to react with perfluorononanoyl chloride to yield fluorinated coronas. After casting from a solvent, the fluorinated particles did not fuse extensively and thus yielded rough coatings on glass slides. Because of the roughness of the coatings, their water and methylene iodide contact angles were large and the contact angle hysteresis was low. In fact, the coatings were superhydrophobic. The water and oil repellence of the coatings improved as the size of the fluorinated coronal bumps increased.

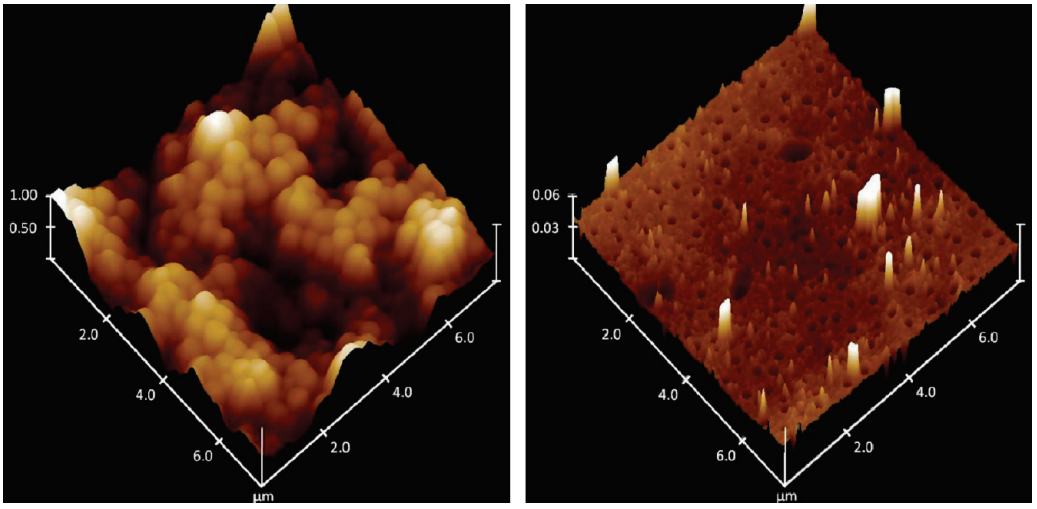

Figure 7. AFM topography images of trifluorotoluene-extracted CSC-2F/epoxy glue (left) and CSC-2F/PCEMA (right) composite coatings.

More interestingly, the remaining hydroxyl groups in the particle coronas were shown to bond covalently with an epoxy glue. The covalently bonded particle layer exhibited similar amphiphobicity as the physically deposited particulate coatings and resisted trifluorotoluene extraction.

AUTHOR INFORMATION

Corresponding Author
*E-mail: guojun.liu@chem.queensu.ca.

ACKNOWLEDGMENT

The Department of National Defence and NSERC of Canada are thanked for sponsoring this research. G.L. thanks the Canada Research Chair Program for a Canada Research Chair Position in Materials Science.

REFERENCES

(1) Lew, C. M.; Li, Z. J.; Li, S.; Hwang, S. J.; Liu, Y.; Medina, D. I.; Sun, M. W.; Wang, J. L.; Davis, M. E.; Yan, Y. S.; Mecerreyes, D.; Alvaro, V.; Cantero, I.; Bengoetxea, M.; Calvo, P. A.; Grande, H.; Rodriguez, J.; Pomposo, J. A. *Adv. Funct. Mater.* **2008**, *18*, 3454–3460.
(2) Ameduri, B.; Boutevin, B.; Kostov, G. *Prog. Polym. Sci.* **2001**, *26*, 105–187.
(3) Feiring, A. E.; Wonchoba, E. R. *Macromolecules* **1998**, *31*, 7103–7104.
(4) Lee, J. R.; Jin, F. L.; Park, S. J.; Park, J. M. *Surf. Coat. Technol.* **2004**, *180*, 650–654.
(5) van Ravenstein, L.; Ming, W.; van de Grampel, R. D.; van der Linde, R.; de With, G.; Loontjens, T.; Thune, P. C.; Niemantsverdriet, J. W. *Macromolecules* **2004**, *37*, 408–413.
(6) Yang, S.; Wang, J. G.; Ogino, K.; Valiyaveettil, S.; Ober, C. K. *Chem. Mater.* **2000**, *12*, 33–40.
(7) Desimone, J. M.; Guan, Z.; Elsbernd, C. S. *Science* **1992**, *257*, 945–947.
(8) Solga, A.; Cerman, Z.; Striffler, B. F.; Spaeth, M.; Barthlott, W. *Bioinspiration Biomimetics* **2007**, *2*, S126–S134.
(9) Furstner, R.; Barthlott, W.; Neinhuis, C.; Walzel, P. *Langmuir* **2005**, *21*, 956–961.
(10) Gao, X. F.; Jiang, L. *Nature* **2004**, *432*, 36–36.
(11) Cassie, A. B. D.; Baxter, S. *Trans. Faraday Soc.* **1944**, *40*, 0546–0550.
(12) Wenzel, R. N. *Ind. Eng. Chem.* **1936**, *28*, 988–994.
(13) Tuteja, A.; Choi, W.; Ma, M. L.; Mabry, J. M.; Mazzella, S. A.; Rutledge, G. C.; McKinley, G. H.; Cohen, R. E. *Science* **2007**, *318*, 1618–1622.
(14) Nosonovsky, M.; Bhushan, B. *J. Phys.: Condens. Matter* **2008**, *20*, 1–6.
(15) Erbil, H. Y.; Demirel, A. L.; Avci, Y.; Mert, O. *Science* **2003**, *299*, 1377–1380.
(16) Feng, L.; Song, Y. L.; Zhai, J.; Liu, B. Q.; Xu, J.; Jiang, L.; Zhu, D. B. *Angew. Chem., Int. Ed.* **2003**, *42*, 800–802.
(17) Feng, L.; Li, S. H.; Li, Y. S.; Li, H. J.; Zhang, L. J.; Zhai, J.; Song, Y. L.; Liu, B. Q.; Jiang, L.; Zhu, D. B. *Adv. Mater.* **2002**, *14*, 1857–1860.
(18) Chen, W.; Fadeev, A. Y.; Hsieh, M. C.; Oner, D.; Youngblood, J.; McCarthy, T. J. *Langmuir* **1999**, *15*, 3395–3399.
(19) Bico, J.; Marzolin, C.; Quere, D. *Europhys. Lett.* **1999**, *47*, 220–226.
(20) Bailey, A. G. *J. Electrostat.* **1998**, *45*, 85–120.
(21) Bravo, J.; Zhai, L.; Wu, Z. Z.; Cohen, R. E.; Rubner, M. F. *Langmuir* **2007**, *23*, 7293–7298.
(22) Motornov, M.; Sheparovych, R.; Lupitskyy, R.; MacWilliams, E.; Minko, S. *Adv. Mater.* **2008**, *20*, 200–05.
(23) Wang, H. X.; Fang, J.; Cheng, T.; Ding, J.; Qu, L. T.; Dai, L. M.; Wang, X. G.; Lin, T. *Chem. Commun.* **2008**, 877–879.
(24) Ofir, Y.; Samanta, B.; Arumugam, P.; Rotello, V. M. *Adv. Mater.* **2007**, *19*, 4075–79.
(25) Cui, X. J.; Zhong, S. L.; Yan, J.; Wang, C. L.; Zhang, H. T.; Wang, H. Y. *Colloids Surf. A* **2010**, *360*, 41–46.
(26) Sawada, H.; Shikauchi, Y.; Kakehi, H.; Katoh, Y.; Miura, M. *Colloid Polym. Sci.* **2007**, *285*, 499–506.
(27) Visintin, P. M.; Carbonell, R. G.; Schauer, C. K.; DeSimone, J. M. *Langmuir* **2005**, *21*, 4816–4823.
(28) Mugisawa, M.; Sawada, H. *Langmuir* **2008**, *24*, 9215–9218.
(29) Moncur, M. V.; Hoo, L. H.; Houghton, E. J. *Transparent Fluorinated Polyurethane Coating Compositions and Methods of Use Thereof*, U.S. Patent No. 6,001,923, 1999.
(30) Thomas, R. R.; Anton, D. R.; Graham, W. F.; Darmon, M. J.; Stika, K. M. *Macromolecules* **1998**, *31*, 4595–4604.
(31) Zheng, G. D.; Stover, H. D. H. *Macromolecules* **2002**, *35*, 7612–7619.
(32) Okubo, M.; Minami, H.; Zhou, J. *Colloid Polym. Sci.* **2004**, *282*, 747–752.
(33) Tanaka, T.; Okayama, M.; Kitayama, Y.; Kagawa, Y.; Okubo, M. *Langmuir* **2010**, *26*, 7843–7847.
(34) Jhaveri, S. B.; Koylu, D.; Maschke, D.; Carter, K. R. *J. Polym. Sci.: A: Polym. Chem.* **2007**, *45*, 1575–1584.
(35) Guerrini, M. M.; Charleux, B.; Vairon, J. P. *Macromol. Rapid Commun.* **2000**, *21*, 669–674.
(36) Jayachandran, K. N.; Takacs-Cox, A.; Brooks, D. E. *Macromolecules* **2002**, *35*, 4247–4257.
(37) Stewart, S.; Liu, G. J. *Chem. Mater.* **1999**, *11*, 1048–1054.
(38) Underhill, R. S.; Liu, G. J. *Chem. Mater.* **2000**, *12*, 3633–3641.
(39) Underhill, R. S.; Liu, G. J. *Chem. Mater.* **2000**, *12*, 2082–2091.
(40) Ming, W.; Wu, D.; van Benthem, R.; de With, G. *Nano Lett.* **2005**, *5*, 2298–2301.
(41) Ciampoli, M.; Nardi, N. *Inorg. Chem.* **1966**, *5*, 41–44.
(42) Ding, J. F.; Liu, G. J. *Macromolecules* **1999**, *32*, 8413–8420.
(43) Guo, A.; Liu, G. J.; Tao, J. *Macromolecules* **1996**, *29*, 2487–2493.
(44) Berne, B. J.; Pecora, R. *Dynamic Light Scattering with Applications to Chemistry, Biology, and Physics*; Dover Publications: Mineola, NY, 1976.
(45) Vogler, E. A. *Adv. Colloid Interface Sci.* **1998**, *74*, 69–117.
(46) Shimizu, R. N.; Demarquette, N. R. *J. Appl. Polym. Sci.* **2000**, *76*, 1831–1845.
(47) Goodwin, J. W.; Ottewill, R. H.; Pelton, R. *Colloid Polym. Sci.* **1979**, *257*, 61–69.
(48) Li, J. Q.; Salovey, R. *J. Polym. Sci.: A: Polym. Chem.* **2000**, *38*, 3181–3187.
(49) Gilbert, R. G. *Emulsion Polymerization: A Mechanistic Approach*; Academic Press: London, 1995.
(50) Dimonie, V. L.; Daniels, E. S.; Shaffer, O. L.; El-Aaser, M. S. In *Emulsion Polymerization and Emulsion Polymers*; Lovell, P. A., El-Aasser, M. S., Eds. John Wiley & Sons Ltd: New York, 1997.
(51) Cho, I.; Lee, K. W. *J. Appl. Polym. Sci.* **1985**, *30*, 1903–1926.
(52) Sundberg, D. C.; Durant, Y. G. *Polymer Reaction Eng.* **2003**, *11*, 379–432.
(53) Slomkowski, S.; Winnik, M. A. *Macromolecules* **1986**, *19*, 500–501.
(54) Coca, S.; Jasieczek, C. B.; Beers, K. L.; Matyjaszewski, K. *J. Polym. Sci.: A: Polym. Chem.* **1998**, *36*, 1417–1424.
(55) Perruchot, C.; Khan, M. A.; Kamitsi, A.; Armes, S. P.; von Werne, T.; Patten, T. E. *Langmuir* **2001**, *17*, 4479–4481.
(56) Tsujii, Y.; Ohno, K.; Yamamoto, S.; Goto, A.; Fukuda, T. *Adv. Polym. Sci.* **2006**, *197*, 1–45.
(57) Aran, B.; Sankir, M.; Vargun, E.; Sankir, N. D.; Usanmaz, A. *J. Appl. Polym. Sci.* **2010**, *116*, 628−635.
(58) Lim, J. M.; Yi, G. R.; Moon, J. H.; Heo, C. J.; Yang, S. M. *Langmuir* **2007**, *23*, 7981–7989.
(59) Ming, W.; Wu, D.; van Benthem, R.; de With, G. *Nano Lett.* **2005**, *5*, 2298–2301.
(60) Zhulina, E. B.; Borisov, O. V.; Priamitsyn, V. A. *J. Colloid Interface Sci.* **1990**, *137*, 495–511.

(61) Zhou, Z. H.; Liu, G. J.; Han, D. H. *ACS Nano* **2009**, *3*, 165–172.
(62) Tsai, P. T.; Yang, Y. M.; Lee, Y. L. *Nanotechnology* **2007**, *18*, 1–7.
(63) Tsai, H. J.; Lee, Y. L. *Langmuir* **2007**, *23*, 12687–12692.
(64) Cao, L. L.; Jones, A. K.; Sikka, V. K.; Wu, J. Z.; Gao, D. *Langmuir* **2009**, *25*, 12444–12448.
(65) Xiu, Y. H.; Zhu, L. B.; Hess, D.; Wong, C. P. *Proceedings of the 56th Electronic Components and Technology Conference*; Institute of Electrical and Electronics Engineers (IEEE): Piscataway, NJ, 2006; pp 686−692.
(66) Du, X.; He, J. H.; Zhao, Y. Q. *J. Phys. Chem. C* **2009**, *113*, 14151 14158.
(67) Qian, Z.; Zhang, Z. C.; Song, L. Y.; Liu, H. R. *J. Mater. Chem.* **2009**, *19*, 1297–1304.
(68) Hong, J.; Bae, W. K.; Lee, H.; Oh, S.; Char, K.; Caruso, F.; Cho, J. *Adv. Mater.* **2007**, *19*, 4364–69.